# A COMPARISON OF FAST FACTORISED BACK-PROJECTION AND WAVENUMBER ALGORITHMS FOR SAS IMAGE RECONSTRUCTION

**A. J. Hunter, M. P. Hayes, P. T. Gough**

Acoustics Research Group, Dept. Electrical and Computer Engineering, University of Canterbury, New Zealand
Email: {a.hunter,m.hayes,p.gough}@elec.canterbury.ac.nz

## Abstract

The Fast Factorised Back-Projection (FFBP) algorithm has received considerable attention recently for SAS image reconstruction. The FFBP algorithm provides a means of trading image quality and/or resolution for a reduction in computational cost over standard Back-Projection. In this paper we describe FFBP for SAS image reconstruction and compare it to the Wavenumber algorithm in terms of computational cost and image quality.

The FFBP algorithm significantly out-performs standard Back-Projection. However, we have found that FFBP is out-performed by the Wavenumber algorithm. Further investigation is required to determine which algorithm is more desirable for motion compensation and multiple-receiver reconstruction.

## Introduction

Synthetic Aperture Sonar (SAS) is an underwater imaging technique that provides higher resolution than conventional side-looking sonar. Moreover, SAS image resolution is independent of range and frequency [1]. The reconstruction of SAS imagery is achieved by synthesizing a larger aperture using a coherent summation of the echo data. SAS image reconstruction is a matched filter operation with the range variant point-spread function of the sonar system. The various different reconstruction algorithms perform this matched filter operation.

The Wavenumber (or Range-Migration) algorithm utilises the Fast Fourier Transform (FFT) to perform the matched filtering in the spatio-temporal frequency domain [2]. Utilisation of the FFT results in a significantly reduced computational cost. Thus, the Wavenumber algorithm has become a popular choice for SAS image reconstruction. Algorithms such as Chirp-Scaling utilise the FFT to similar effect. The FFT-based algorithms require regularly sampled echo data. Therefore, reconstruction from an arbitrary collection geometry is non-trivial. Reconstruction from multiple-receivers and motion compensation is challenging using such algorithms.

The Back-Projection algorithm does not require regularly sampled echo data and is well-suited for reconstruction from an arbitrary collection geometry. However, Back-Projection is much slower than the FFT-based algorithms [3]. Recently, a modification of the Back-Projection algorithm was proposed. Fast Factorised Back-Projection provides a means of trading image quality and/or resolution for a reduction in computational cost over standard Back-Projection [4].

In this paper, the FFBP algorithm is described and compared to the Wavenumber algorithm in terms of computational cost and image quality. Computational cost is determined theoretically and image quality is determined from images reconstructed with our implementation of the FFBP and Wavenumber algorithms on data simulated with the parameters of our Kiwi-SAS system. We have found that the FFBP algorithm significantly out-performs standard back-projection, but is out-performed by the Wavenumber algorithm.

## Back-Projection

The Back-Projection algorithm has been used extensively for Computed Tomography (CT) in Medical Imaging. It has since been adapted for the SAR/SAS imaging geometry [3]. The algorithm operates by *back-projecting* each range data-sample along an arc in the reconstructed image. Each arc corresponds to a spherical shell centered at the given aperture position with a radius corresponding to the given range. Reconstruction is achieved since targets interfere constructively at the points where the back-projected arcs coincide.

The back-projected image $s'(x, y)$ is given by

$$s'(x, y) = \int_{-\infty}^{\infty} d(r, y') \exp(j2k_c r)\, r\, dy', \quad (1)$$

where $d(x, y)$ is the baseband echo data, $k_c = 2\pi f_c/c$ is the wavenumber of the carrier, and

$$r = \sqrt{x^2 + (y' - y)^2}. \quad (2)$$

A further filtering step is required to yield the reconstructed image

$$s(x, y) = h(x) \star s'(x, y), \quad (3)$$

where $\star$ denotes convolution and

$$h(x) = \int_{-\infty}^{\infty} |u| \exp(j2\pi x\, u)\, du. \quad (4)$$
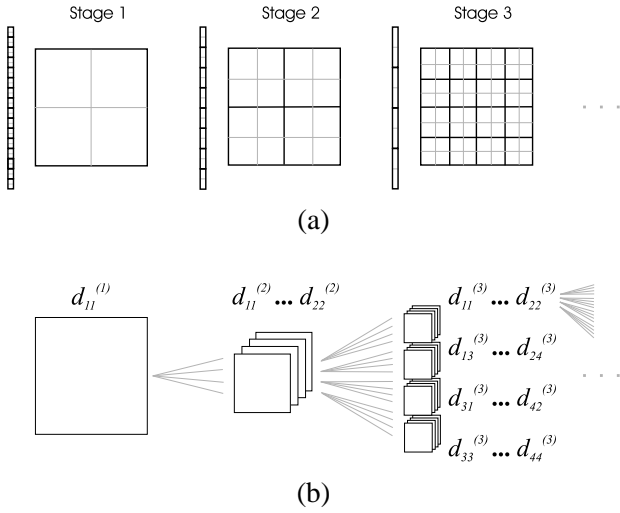
(a)



(b)

Figure 1: The FFBP algorithm achieves a reduction in computational complexity by recursive factorisation and decimation of the echo data. An example factorisation is shown in (a), the resultant hierarchy of data-sets is shown in (b).

Back-Projection is computationally expensive with a computational cost of order $M \times N \times P$ for $P$ aperture positions and a reconstructed image of size $M \times N$ pixels. The Back-Projection algorithm is slow compared to the Wavenumber algorithm, which achieves a computational cost of order $M \times N \times log_2(P)$ by utilisation of the FFT [3]. However, Back-Projection does have some advantages. In particular, it lends itself easily to arbitrarily sampled collection geometries (assuming adequate sampling), which is useful for reconstruction from multiple receivers and for motion compensation.

**Fast Factorised Back-Projection**

The Fast Factorised Back-Projection algorithm (FFBP) was recently developed for CT and adapted for SAR/SAS [4]. FFBP provides a means of trading image quality and/or resolution for a reduction in computational cost. The algorithm is performed in two parts: 1) The echo data is recursively factorised into a number of decimated data-sets for subimages of the reconstructed image, 2) Each data-set is back-projected to the corresponding subimage. A computational gain is achieved through decimating the data in the factorisation step. However, doing so introduces an error that degrades the image quality.

The echo data is factorised in a number of stages. At each stage the reconstructed image is further subdivided into smaller subimages with corresponding data-sets $d_{mn}^{(s)}$ as shown in Fig. 1. The superscript $(s)$ denotes the stage and the subscript $mn$ is the index of the subimage. The data-set for a given subimage $mn$ in the
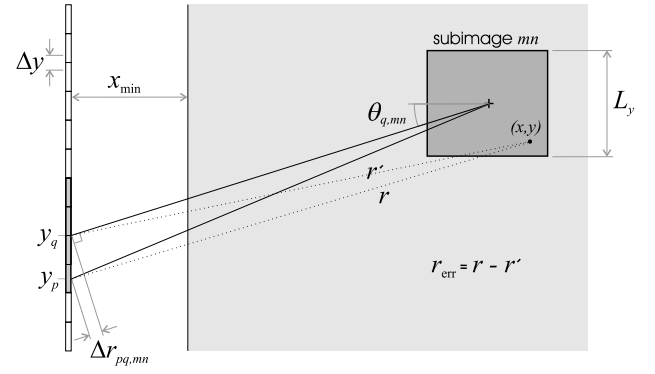


Figure 2: At each stage of the FFBP algorithm, groups of along-track samples (from the appropriate data-set in the previous stage) are combined and focused to the centre of each subimage. This introduces a far-field approximation error $r_{\mathrm{err}}$.

current stage $s$ is given by

$$d_{mn}^{(s)}(x, y_q) = \sum_{p=qQ}^{(q+1)Q-1} d_{m'n'}^{(s-1)}(x - \Delta r_{pq,mn}, y_p)$$
$$\times \exp(jk_c \Delta r_{pq,mn}), \quad (5)$$

where $d_{m'n'}^{(s-1)}$ is the data-set for the subimage in the previous stage that contains the subimage $mn$. The along-track samples are combined such that the data is focused at the subimage centre.

$$\Delta r_{pq,mn} = (y_p - y_q)\sin\theta_{q,mn}, \quad (6)$$

is the delay required to focus at the centre of the subimage $mn$, where $\theta_{q,mn}$ is the angle from $y_q$ to the subimage centre. The along-track sample rate is decimated by the factor $Q$ and the new sample positions are given by

$$y_q = \frac{1}{Q}\sum_{p=qQ}^{(q+1)Q-1} y_p. \quad (7)$$

This is illustrated in Fig. 2. Fewer range samples are required for each data-set as the subimages decrease in size. This combined with the along-track decimation of the data gives the FFBP algorithm its computational gain.

A far-field approximation error is introduced at each stage of the algorithm when combining subsequent along-track samples as described by (5). The approximation error $r_{\mathrm{err}}$ is illustrated in Fig. 2 and the maximum bound of this error is given by [5]

$$|r_{\mathrm{err}}| < \frac{\Delta y\, L_y}{4\, x_{\min}} \quad (8)$$

for a linear collection geometry, where $\Delta y$ is the along-track sample spacing, $L_y$ is the size of the subimage

in the along-track dimension, and $x_{\min}$ is the minimum range of the reconstructed image. The approximation error at each stage determines the quality of the reconstructed image and the computational gain.

At the final stage of the algorithm each data-set is back-projected to the corresponding subimage (as described in the previous section) yielding the reconstructed image. Ideally, at this stage each subimage is a single pixel with dimensions of the maximum system resolution and the back-projection step is trivial. Similarly, at any intermediate stage the data-sets can be low-pass filtered (to prevent aliasing) and back-projected to pixels with dimensions of the subimage yielding a lower resolution reconstruction.

*Computational Cost*

The computational cost of FFBP is largely dependent on the desired image quality and the choice of factorisation. At each stage the computational cost of factorising the data is given by

$$C^{(s)} = N_{mn}^{(s)} \times N_x^{(s)} \times N_y^{(s)}, \qquad (9)$$

where $N_{mn}$ is the number of subimages, and $N_x$ and $N_y$ are the number of range and along-track samples per subimage data-set. The computational cost of the final back-projection step is given by

$$C_{bp} = N_{mn}^{(S)} \times M^{(S)} \times N^{(S)}, \qquad (10)$$

where $M$ and $N$ are the number of range and along-track image pixels per subimage at the final stage $S$. The total computational cost is given by

$$C = \sum_{s=1}^{S} C^{(s)} + C_{bp}. \qquad (11)$$

**Results**

Two performance factors were compared between the FFBP and Wavenumber algorithms: computational cost and image quality. The theoretical computational cost (detailed in the previous section) was used to compare the two algorithms since a direct comparison of the algorithm implementations would be biased by coding efficiencies. In particular, the Wavenumber algorithm has a clear advantage due to the use of highly optimised FFT code. The comparison of image quality was assessed by simulating ideal point-targets and comparing the reconstructed imagery obtained using our implementations of the algorithms.
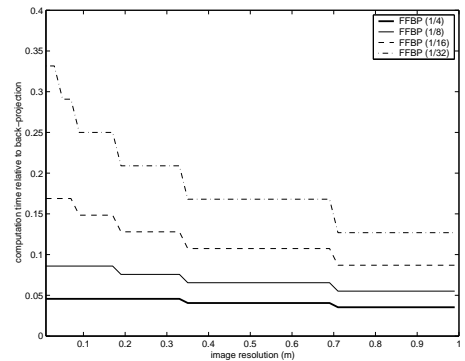
The minimum computational cost of the FFBP algorithm is shown in Fig. 3 for varying image and algorithm parameters. The $M \times N \times \log_2(P)$ cost of the Wavenumber algorithm is assumed. Here we have demonstrated that FFBP is more efficient than standard
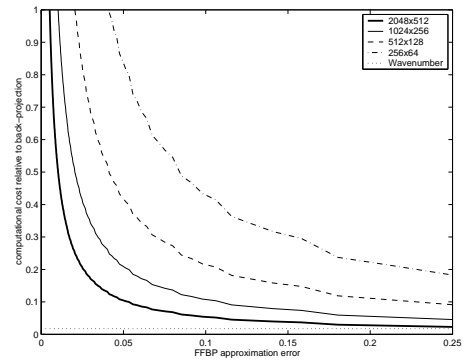


(a)
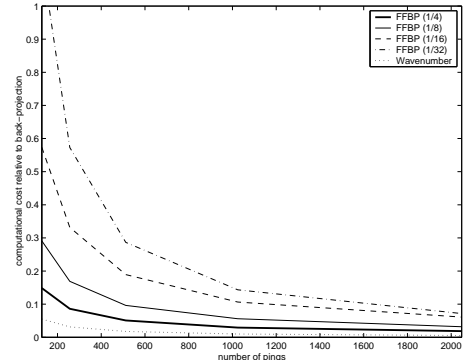


(b)



(c)

Figure 3: Computational cost of the FFBP and Wavenumber algorithms normalised with respect to standard back-projection for varying (a) approximation error, (b) number of pings, and (c) image resolution (number of stages)

Back-Projection and approaches the computational efficiency of the Wavenumber algorithm for large approximation errors of order $\lambda/4$. The efficiencies of both the Wavenumber and FFBP algorithms increase with the number of pings and image size. The computational cost of FFBP can be further reduced by truncation of the factorisation step and back-projection to a lower resolution image.

Echo data for a line of point-targets was simulated using the parameters of the Kiwi-SAS system [6]. The images reconstructed using our implementations of the

FFBP and Wavenumber algorithms are shown in Fig. 4. The FFBP algorithm with a low approximation error of $\lambda/32$ yields similar quality imagery to the Wavenumber algorithm. Both algorithms accurately reconstruct the image. However, for larger approximation errors the quality of the FFBP imagery degrades quickly. At an approximation error of $\lambda/4$ most of the energy is contained in the *sidelobes* of the reconstructed targets.

## Conclusions

The FFBP and Wavenumber algorithms have been compared in terms of computational cost and image quality. We have found that FFBP only achieves computational efficiency comparable to the Wavenumber algorithm for large images and significant degradation in image quality. The Wavenumber algorithm outperforms FFBP in this respect. However, further research is required to determine if FFBP is more suited to multiple-receiver reconstruction and motion compensation.

## Acknowledgment

Alan Hunter thanks the University of Canterbury for his Doctoral Scholarship.

## References

[1] D. W. Hawkins, Synthetic Aperture Imaging Algorithms: with application to wide bandwidth sonar. PhD thesis, Department of Electrical and Electronic Engineering, University of Canterbury, October 1996.

[2] W. G. Carrara, R. S. Goodman, and R. M. Majewski, Spotlight Synthetic Aperture Radar Signal Processing Algorithms. 1995.

[3] M. D. Desai and W. K. Jenkins, "Convolution backprojection image reconstruction for spotlight mode synthetic aperture radar," IEEE Trans. Image Processing, vol. 1, pp. 505–517, October 1992.

[4] S. Xiao, D. C. Munson, Jr., S. Basu, and Y. Bresler, "An $N^2 \log N$ back-projection algorithm for SAR image formation," in Thirty-Forth Asilomar Conference on Signals, Systems, and Computers, October 2000, vol. 1, pp. 3–7.

[5] S. M. Banks, Studies in High Resolution Synthetic Aperture Sonar. PhD thesis, University College London, UK, September 2002.

[6] P. J. Barclay, M. P. Hayes, and P. T. Gough, "Reconstructing seafloor bathymetry with a multichannel broadband InSAS," in OCEANS 2003, San Diego, CA, September 2003, IEEE.
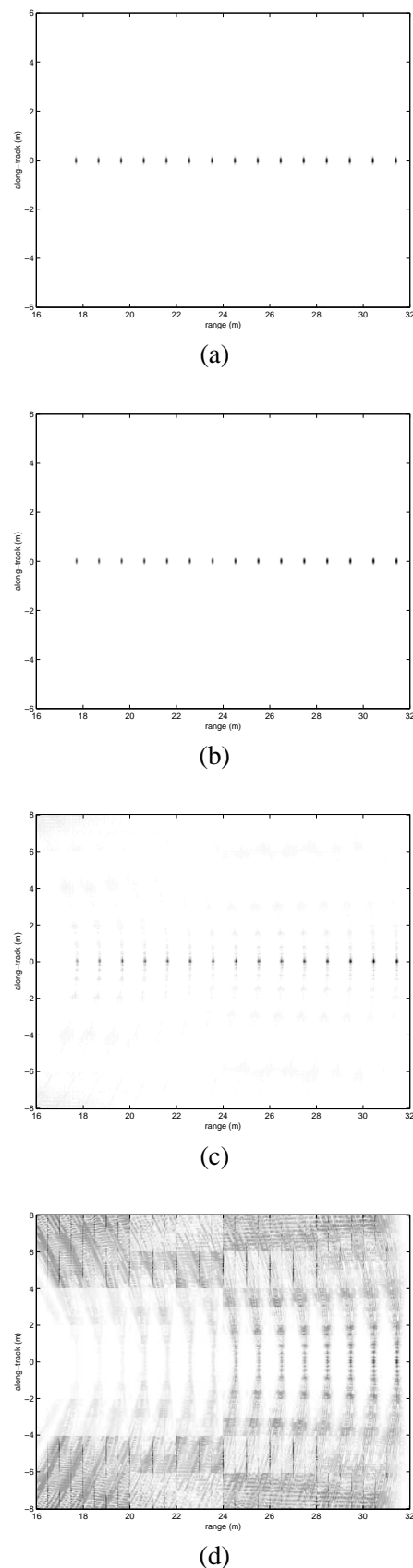
(a)



(b)



(c)



(d)

Figure 4: Reconstructed imagery of a line of point targets simulated using the parameters of the Kiwi-SAS system and reconstructed using (a) Wavenumber algorithm, (b) FFBP ($\lambda/32$ error), (c) FFBP ($\lambda/8$ error), (d) FFBP ($\lambda/4$ error).